Manganite reduction by *Shewanella putrefaciens* MR-4

INGA LARSEN,[1] BRENDA LITTLE,[2] KENNETH H. NEALSON,[1,3,]* RICHARD RAY,[2] ALAN STONE,[4]
AND JUIHAN TIAN[4]

[1]Center for Great Lakes Studies, 600 E. Greenfield Ave., Milwaukee, Wisconsin 53204, U.S.A.
[2]Naval Research Laboratory, Code 7333, Stennis Space Center, Mississippi 39529-5004, U.S.A.
[3]Jet Propulsion Laboratory, California Institute of Technology, MS183-301, 4800 Oak Grove Drive, Pasadena,
California 91109-8009, U.S.A.
[4]Department of Geography and Environmental Engineering, Johns Hopkins University,
408 Ames Hall, Baltimore, Maryland 21218, U.S.A.

ABSTRACT

Previous studies have documented dissimilatory growth of bacteria on solid Mn^{4+} oxide, but Mn^{3+} oxides have not been previously studied; here we have demonstrated for the first time the bacterial reduction of manganite. Strain MR-4 of *Shewanella putrefaciens* was able to grow on and rapidly reduce insoluble needle-shaped crystals of synthetic manganite (MnOOH), converting them to soluble Mn^{2+} in the process. The rate of Mn^{3+} reduction was optimal at pH of 7.0 and 26 °C consistent with an enzymatic reaction. In addition the rates of reduction were in proportion to the amount of manganite added, but nearly independent of the cell concentration present (e.g., cell number had only a small effect on the rate of Mn^{3+} reduction at early stages of growth) suggesting that surface properties were dictating the rates of metal reduction. This thesis was supported by major differences in reduction rates when Mn oxides of different surface areas were studied. Removal of the carbon source (formate or lactate) or addition of metabolic inhibitors reduced the rate of metal reduction. No Mn^{3+} reduction was observed when the samples were oxygenated, nor when the cells were separated from the Mn^{3+} oxide by a dialysis membrane. Environmental scanning electron microscopy (ESEM) images showed close contact of the cells with the needle-shaped crystals during early stages of reduction. In later stages, the closely associated cells were coated with a layer of extracellular polymeric material that obscured the cells when viewed by ESEM. When manganite crystals were dried and gold coated, and viewed by standard scanning electron microscopy (SEM), abundant bacteria could be seen on the surface of the metal oxide in a thin biofilm-like layer. The layer of extracellular polymer is a new finding, and neither the composition, function, nor importance in the manganese reduction process have been elucidated.

INTRODUCTION

Bacteria capable of dissimilatory growth on oxidized manganese were first described by Myers and Nealson (1988a) and Lovley and Phillips (1988). In the former report, the bacteria, identified as *S. putrefaciens,* were shown to grow on solid Mn^{4+} oxides, using lactate as the carbon source. Mn^{4+} reduction required cell contact and was inhibited by oxygen as well as several metabolic inhibitors. Subsequent studies showed that both Fe^{2+} produced from ferric iron reduction or H_2S, produced by thiosulfate reduction could also reduce Mn^{4+} oxide, leading to an indirect reduction of MnO_2 by chemical intermediates (Myers and Nealson 1988b). Thus, the ability of *S. putrefaciens* to reduce other compounds like Fe^{3+}, thiosulfate, or elemental sulfur (Moser and Nealson 1996) results in products that cause rapid Mn^{4+} reduction and

obscure the measurement of direct (enzymatic) manganese reduction (Nealson and Saffarini 1994).

Several mineral forms of insoluble Mn^{4+} oxides of the general formula MnO_2 were shown previously to be reduced at quite different rates (Burdige et al. 1992), such that amorphous oxides with high surface area are the most reactive, while highly crystalline, low surface area oxides like pyrolusite are almost totally inert to bacterial reduction. For Mn^{4+} oxides, surface area is a very important parameter, although almost certainly not the only factor controlling reduction rate. In studies of soluble Mn^{3+} pyrophosphate, Kostka et al. (1995), reported the stability of some Mn^{3+} containing ligands and the ability of *S. putrefaciens* to reduce the bound Mn^{3+} to soluble Mn^{2+}.

Mn^{3+} oxides can be readily reduced by any of a variety of organic compounds that were also capable of reducing Mn^{4+} oxides (Bricker 1965; Stone and Morgan 1984a, 1984b; Stumm and Giovanoli 1965; Xyla et al. 1992). In

---

contrast, no studies of the microbial reduction of Mn^{3+}-containing oxides were found.

Manganite is a Mn^{3+}-containing manganese oxide of the general formula MnOOH, and its distribution in ore bodies is well documented in the literature (Hewett and Fleischer 1960; Hewett 1966). However, its distribution in aquatic environments is not well documented, and in general, the dynamics of Mn^{3+} oxidation or reduction are not extensively studied. Here we present an initial report of microbial reduction of synthetic manganite by *S. putrefaciens* MR-4. As with the other oxidized Mn compounds, efficient reduction of Mn^{3+} depends on anaerobic conditions, exhibits pH and temperature (*T*) optima consistent with an enzymatic process, is sensitive to metabolic inhibitors and poisons, and requires cell contact. In addition, a visible biofilm forms during manganese reduction; this biofilm appears to isolate the bacteria and the oxide surface from the bulk environment.

EXPERIMENTAL METHODS

Bacteria and media

Manganese reduction experiments with *S. putrefaciens*, strain MR-4, were performed in a defined medium (M1), using lactate (30 m*M* final) as the carbon source (Myers and Nealson 1988). The basic components of the medium were: 0.95 g NH_4Cl; 100 mL basal salts solution (recipe shown below); 875 mL dH_2O (deionized water); 0.1 mL metals supplement; and 0.2 mL 0.115 *M* Na selenate. The pH was adjusted to 7.4 and the medium autoclaved for 20 min. To this medium the following were added: 10 mL sterile 0.2 *M* Na bicarbonate and 15 mL phosphate solution (added via sterile filtration to prevent formation of white precipitate). To individual flasks/tubes other additions were made (per 100 mL media): 3 mL 1 *M* lactate; 0.25 mL sterile 10% (w/w) CAA (acid hydrolyzed casamino acids)—only added to growth (not experimental) cultures. Manganese oxides were added as specified in the text.

To prepare the basal salts mixture for stock solutions, the following components were completely dissolved in 800 mL dH_2O, 2 g $MgSO_4 \cdot 7H_2O$, 0.57 g $CaCl_2 \cdot 2H_2O$, 0.2 g EDTA, disodium, 0.012 g $FeSO_4 \cdot 7H_2O$. 10 mL of trace elements stock solution was added, and the volume brought to 1000 mL: the medium was filter sterilized and stored at 4 °C.

Phosphate solution (stored at 4 °C) consisted of: 30 g KH_2PO_4; 66.1 g K_2HPO_4; 800 mL dH_2O with the pH adjusted to 7.4 and the volume adjusted to 1 L. Metals supplement consisted of: 1.41 g $CoSO_4 \cdot 7H_2O$; 1.98 g $Ni(NH_4)_2(SO_4)_2 \cdot 6H_2O$; 0.58 g NaCl; 100 mL dH_2O. The metals supplement was autoclaved for 20 min and stored at 4 °C. The trace elements solution contained, per liter of distilled water: 2.8 g H_3BO_3; 0.24 g $ZnSO_4 \cdot 7H_2O$; 0.75 g $Na_2MoO_4 \cdot 2H_2O$; 0.042 g $CuSO_4 \cdot 5H_2O$; 0.17 $MnSO_4 \cdot H_2O$. It was filter sterilized and stored in glass at 4 °C.

Bacterial inoculum

Before each experiment, cells were transferred from nutrient agar plates to liquid media tubes and incubated for ~8–10 h at room temperature. Subsequently, the culture was diluted 1:100, incubated overnight and again diluted 1:25 and incubated for 6–8 h. Incubations were maintained under anaerobic conditions at 30 °C. Successive transfers insured that cells were (1) acclimated to liquid media and (2) in exponential growth phase at the start of each experiment [this was assured by diluting the cells to below an optical density at 550 nm (OD_{550}) of 0.01, and retransferring before the cells reached an OD_{550} of 0.3]. After the final incubation period, cells were harvested by centrifugation and resuspended in fresh M1 medium. Neither the resuspension medium nor the medium used in any of the experiments contained CAA, which were only added to media used to grow cells before the experiments. During preliminary experiments, enhanced growth of *S. putrefaciens* in media containing CAA was observed (data not shown). Cell density of the resuspension was determined by direct counting using epifluorescence microscopy (Clesceri et al. 1989; Porter and Feig 1980). Cells were fixed by a 1:10 dilution into a 0.5% solution of glutaraldehyde, stained with DAPI (4′,6-diamidino-2-phenylindole, Sigma Chemical Co.) at a final concentration of 1 μg/mL^{-1}, and counted in an Axiolab microscope (Carl Zeiss, Inc.).

Manganite reduction experiments

All experiments, except those described below, were performed in open 250 mL Erlenmeyer flasks inside a Coy anaerobic chamber containing an atmosphere of 10% hydrogen and 90% nitrogen (27 °C). Prior to inoculation, media in flasks were equilibrated in the anaerobic hood for at least 24 h. Initially, two experiments were run to examine the effects of different concentrations of cells and MnOOH on Mn reduction rates. Only a single factor was varied in each experiment. Experiments were also run with several control treatments (no carbon, no cells, killed cells, no cell/oxide contact, outside the hood), inhibitors (1m*M* azide, 0.2 m*M* cyanide, 0.05 m*M* 2 heptyl-4 hydroxyquinoline n-oxide (HQNO), 0.1 m*M* carbonyl cyanide m-chlorophenyl hydrazone (CCCP) and Mn oxides (birnessite, pyrolusite). Unless otherwise noted, experimental flasks were inoculated to a final concentration of 5×10^6 cells/mL and 200 μ*M* MnOOH. At various intervals after inoculation, three 1 mL samples were removed from each flask and filtered (0.2 μm pore size) into acid washed 1.5 mL plastic Eppendorf tubes. Each sample was acidified with 10 μL concentrated nitric acid and refrigerated until analysis.

Effects of pH and *T* on manganite reduction were tested in 50 mL sterile serum bottles sealed with rubber septa and an aluminum crimp seals. Temperature treatments were 4, 27, 37, and 44 °C and the pH treatments were 4, 5, 7.4, and 8.5. Because of the abiotic dissolution of solid Mn compounds at low pH, biotic and abiotic reduction rates were measured in separate serum bottles for each acidic pH. In these low pH experiments, only one serum bottle was inoculated with cells, to compare biological and chemical reduction and assess net biological activity

at different pH values. The pH and temperature vials were sampled at two discrete time points, and no attempt was made to perform a more resolved time course analysis.

Determination of Mn²⁺

Mn²⁺ was determined by atomic absorption spectrometry (AAS) using an air-acetylene flame. Three readings were taken at 1 s intervals for each sample. Relative standard deviations for intra-sample analyses were usually <3%. Inter-sample variance measured in triplicates taken from each flask generally yielded relative standard deviations <5%. In addition, one treatment containing 5×10^6 cells/mL and 200 μM MnOOH was run through each experiment and showed very good replication (Fig. 1).

During Mn²⁺ analyses, standards made in distilled water ($+10$ μL HNO$_3^-$ mL^{-1}) were used to calibrate the atomic absorption spectrometer. Media blanks, run periodically during the analyses, yielded a concentration of ~1.3 μM. This value was subtracted from each sample to give the final Mn²⁺ concentration. Although standards made in water were stable, those made in media decreased with time despite the fact they were acidified to pH < 1. Over a period of several days, the Mn²⁺ concentration in the media standards decreased by as much as 10% compared to standards in distilled water (data not shown). No significant decay was observed when media standards were made in the anaerobic hood, and treated and sampled as described above for Mn reduction experiments.

Preparation of manganese oxides

Manganite was prepared according to Stumm and Giovanoli (1976) as follows: 20.4 mL of a 30% (8.82 M) solution of H$_2$O$_2$ solution was added to 1000 mL of 0.06 M MnSO$_4$ at room temperature and, with vigorous stirring, 300 mL of 0.2 M NH$_3$ was added. The solution was quickly heated to the boiling point, and then maintained at 95 °C for 6 h. While keeping the product hot, it was separated from solution and rinsed with four 250 mL portions of hot water. Two additional cold water washes employed using resuspension/centrifugation for the washing, and the final suspension was frozen until used. Birnessite and pyrolusite were obtained from David Burdige, and they are identical to those described in previous experiments (Burdige et al. 1992).

ESEM sample preparation and instrument operation

Two milliliter samples of manganite were removed from the anaerobic vials using an Eppendorf pipette, and dispensed into two centrifuge tubes with 15 mL distilled water to remove residual culture medium from mineral surfaces before fixation. Suspensions were centrifuged gently (3000 rpm in a tabletop centrifuge) for 2 min to precipitate the solid particles, the supernatant decanted, and the rinse procedure repeated. One milliliter of sample with residual rinse water was removed and fixed in 0.1 M Na cacodylate buffer (pH = 7.2) containing 2 wt% (final concentration) glutaraldehyde. This procedure was
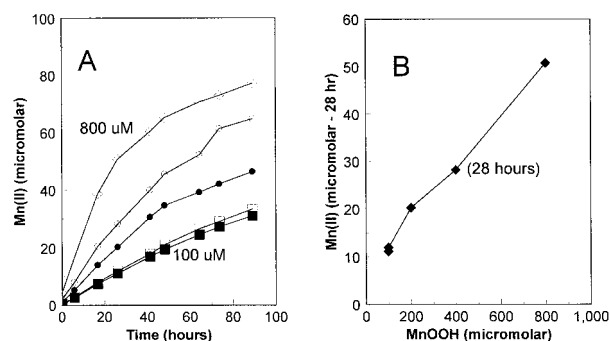

FIGURE 1. Rates and extents of manganese reduction as a function of amount of manganite present. In this experiment, cell number was constant in all cases, while manganite was added at different concentrations, over a range of 100 to 800 μM. (**A**) Mn reduction (appearance of Mn²⁺ as a function of time) for each concentration of manganite. The closed and open squares represent two separate experiments done with 100 μM manganite; closed circles = 200 μM manganite; open circles = 400 μM, and open diamonds = 800 μM. (**B**) Manganite reduction after 28 h as a function of manganite concentration. After 28 h, an eight-fold increase in substrate level yields approximately a five-fold increase in the extent of manganite reduction.

repeated at timed intervals (24, 48, 66, 72, 90, and 190 h). Samples remained in the fixative for a minimum of 4 h, but usually overnight. Fixative was removed using the same rinsing procedure described above. Five microliters of the fixed, rinsed samples were extracted and placed directly into a counterbore (0.1 × 0.04 cm deep) specimen mount of a Peltier cooling device in the ESEM chamber. The ESEM (Electroscan Corporation, Wilmington, Massachusetts) uses a secondary electron detector capable of forming high resolution images (50 Å) at pressures in the range of 0.1 to 20 torr. At these relatively high pressures, specimen charging is dissipated into the gaseous environment of the specimen chamber, enabling direct observation of uncoated, nonconductive specimens. If water vapor is used as the specimen environment, wet samples can be observed. Samples were imaged at 20 kev with temperature (4 °C) and chamber vapor pressure (4 torr) controlled so that condensation would keep samples moist. Coordinates were recorded for each subarea examined in detail.

Specimens were removed from the ESEM, dehydrated through a series of acetone/xylene washes, dried, sputter-coated with gold (20 nm thickness) using a Polaron (Line Lexing, PA) series II sputtering system, Type E5100, and reexamined using the ESEM as a traditional SEM at an accelerating voltage of 30 kev and a vacuum of 10^{-5} torr. After removal of the specimen from the ESEM, sample preparation, and replacement in the specimen chamber, subareas could be precisely relocated using previously recorded x-y coordinates.

Surface area estimations

Surface areas of birnessite and pyrolusite were determined previously (Burdige et al. 1992), and the SA of
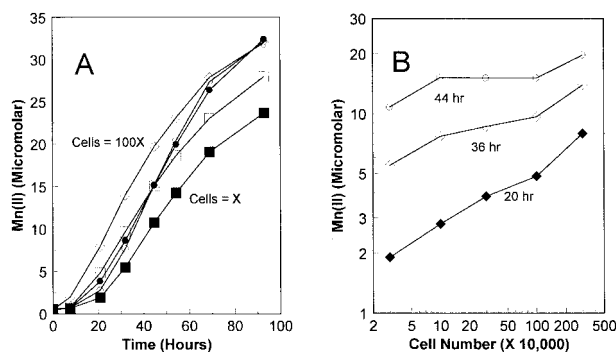
FIGURE 2. Rates and extents of manganese reduction as a function of cell number. Manganite concentration was constant at 200 μM, while cell number was varied over a factor of 100. (**A**) Manganite reduced (Mn^{2+} produced) as a function of time: closed squares = X (3×10^4 cell/mL final concentration); open circles = 3×; closed circles = 10×; open squares = 30×; and open diamonds = 100×. (**B**) Extent of manganite reduction as a function of cell number at various times: closed triangles = 20 h; open triangles = 36 h; and open circles = 44 h. A 100-fold increase in cell number yields only a two- to three-fold increase in manganite reducing ability during the early stages of the experiment, indicating that surface limitation is an important parameter.

FIGURE 3. Rates of manganite reduction under different experimental conditions. This experiment utilized 200 μM manganite, and 5×10^6 MR-4 cells/mL. The closed circles indicate the Mn^{2+} produced by the untreated positive control, while the closed triangles indicates a series of negative controls including no cell addition, heat killed cells, and cells treated with HgCl$_2$. Cells treated with CCCP as described in the text (asterisk) show very low levels of Mn^{2+} production, as do cells exposed to molecular oxygen (open circles) and cells isolated from the manganite by the use of dialysis membranes (closed squares). The no-carbon control (closed stars) shows a rapid rate of reduction for about 44 h, after which the rate of manganite reduction appears to dramatically decrease.

manganite in these experiments was estimated by electron microscopic analysis in relation to these two standards.

RESULTS

Reduction of manganite by MR-4

Rates of reduction are strongly dependent on manganite concentration (Fig. 1A.) The process is not directly proportional: for an eight-fold increase in MnOOH, a five-fold increase in Mn^{2+} production rate is noted (Fig. 1B). Eventually, all of the MnOOH was reduced by the bacteria, irrespective of manganite concentration (data not shown).

When MnOOH content is constant and cell number is varied, a different pattern is seen (Fig. 2). High cell numbers increase the reduction slightly in the early stages (Fig. 2A), but as shown, even a 300-fold increase in cell number results in only a two- to three-fold increase in rate of metal reduction at 21 and 36 h (Fig. 2B), and after this time there is little correlation between inoculum size and the amount of Mn^{2+} produced. After 48 h, there is no effect of cell number on Mn^{3+} reduction.

Several variables were tested for their effect on MnOOH reduction (Fig. 3). The control sample receiving no treatments showed good reduction, as in the experiments of Figures 1 and 2, and the no-carbon control showed reduction that increased for the first 48 h and then leveled off. All other treatments effectively stopped MnOOH reduction. These included: (1) enclosing the MnOOH in a dialysis bag to prevent cell/oxide contact; (2) incubation in the presence of oxygen; (3) inoculation with heat-killed cells (control); (4) introduction of CCCP; and (5) uninoculated control.
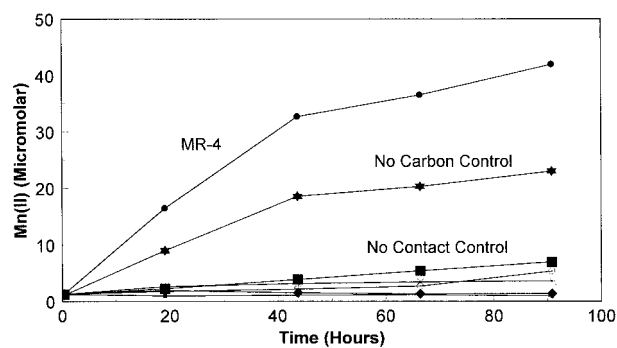
Using similar amounts (200 μM) of different manganese oxides, the rates of reduction of manganite, birnessite, and pyrolusite were compared (Fig. 4). The rate of reduction for manganite is intermediate between birnessite and pyrolusite (Fig. 4). In previous studies, Burdige et al. (1992), using the same oxides showed that rates of Mn oxide dissolution for various Mn^{4+} oxides were proportional to surface area, with the birnessite having a surface area of 45 m^2/g, and pyrolusite an area of nearly 1000-fold less. Electron microscopic images of manganite yield an estimate of between 0.9 and 2.5 m^2/g for the manganite in these experiments. The variability derives from variations seen in manganite crystals in separate fields that were viewed. These estimates of surface area
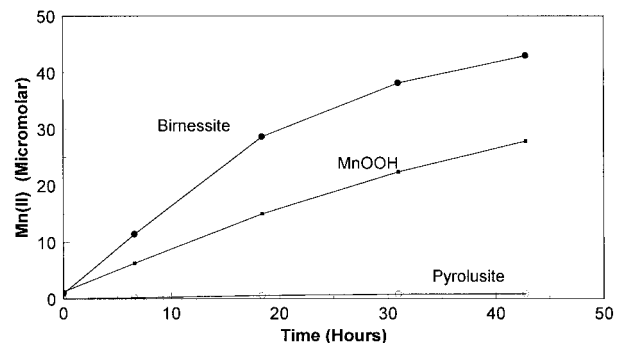

FIGURE 4. Rates of Mn^{2+} production when different Mn oxides are used. These experiments were begun with equimolar amounts of three different Mn oxides. All were adjusted to 200 μM and identical numbers (5×10^6) of MR-4 cells were added to each.

TABLE 1. Manganite reduction by *S. putrefaciens* MR-4

Variable	Amount	Experimental μM Mn²⁺ ± (SD)	Control μM Mn²⁺ ± (SD)	Net reduction μM Mn²⁺ ± (SD)
T	4 °C	9.1 (0.02)	1.1 (0.01)	8.0 (0.02)
T	26 °C	22.9 (0.18)	1.3 (0.02)	21.6 (0.15)
T	37 °C	14.4 (0.06)	1.5 (0.01)	13.9 (0.05)
T	44 °C	6.9 (0.05)	1.9 (0.01)	5.0 (0.05)
pH	4.0	101.3 (2.0)	103.1 (2.4)	–
pH	5.0	39.4 (0.4)	44.0 (1.1)	–
pH	7.4	12.2 (0.04)	1.2 (0.01)	11.0 (0.02)
pH	8.5	4.7 (0.09)	0.4 (0.004)	4.3 (0.02)
Inhibitor	Oxygen	4.4 (0.03)	–	89.1%
Inhibitor	HQNO	37.8 (0.4)	–	6.3%
Inhibitor	HgCl₂	3.2 (0.02)	–	92.1%
Inhibitor	CCCP	2.8 (0.01)	–	93.1%
Inhibitor	Cyanide	40.1 (0.5)	–	0%

Notes: The left columns show conditions of temperature, pH, or inhibitors added. For all experiments, the starting cell number was 5×10^6 cells/mL and the MnOOH concentration was 200 μM. The control column for pH and temperature indicates that no cells were present. For the inhibitor experiments, comparison is made to experimental with no inhibitor present, which results in 40.3 (0.5) μm Mn²⁺. The reduction column gives the difference from 40.3 μM Mn²⁺. Micromolar concentration as percentage inhibition.

are consistent with estimates of surface area made via comparisons of the relative surface areas of the minerals. Because the crystal shape and morphologies, and presumably the crystallinities of the three oxides are quite different, there is a need for a detailed study of the factors (in addition to surface area) that limit the rate of microbial reduction.

The effect of inhibitors and some selected pH and temperature conditions on the relative amounts of Mn²⁺ produced is shown in Table 1: CCCP, mercuric chloride, and molecular oxygen prevented Mn³⁺ reduction, while other inhibitors had only minor effects.

ESEM imaging during manganite reduction

During the reduction of MnOOH, samples were taken for analysis by ESEM and SEM to determine the spatial relationship between cells and metal oxides. Figure 5 shows an ESEM image of the uninoculated control MnOOH—images taken with SEM reveal a similar structure (not shown). In contrast, after approximately 72 h, when reduction is approximately 25% complete (Fig. 6), images from the two microscopes are very different. It is difficult to resolve either the surface of the metal oxide or bacterial cells in the ESEM image (panels A and C). In contrast SEM images of vacuum dried samples (panels
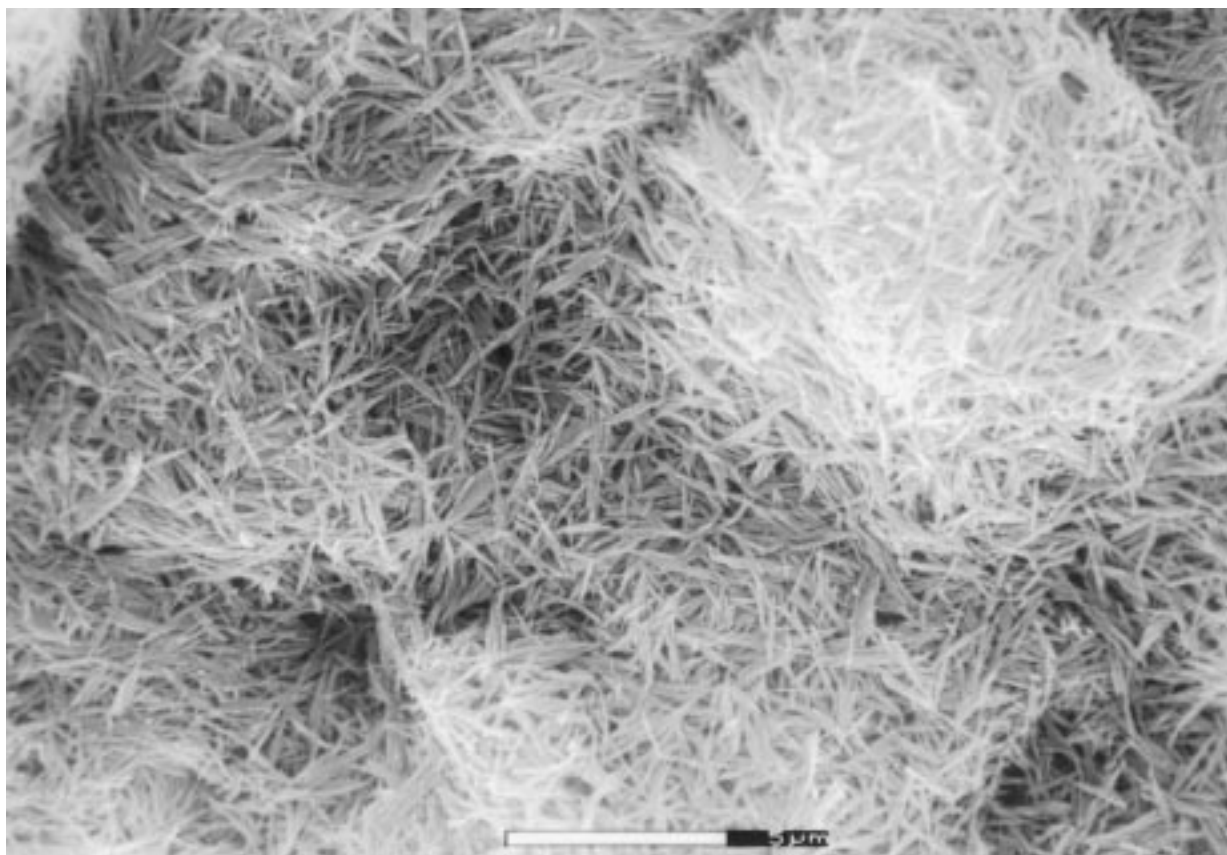

FIGURE 5. ESEM (Environmental Scanning Electron Microscope) image of the uninoculated manganite as a wet sample. A higher magnification image of uninoculated manganite is shown in Figure 7A. Bar = 5 μm.
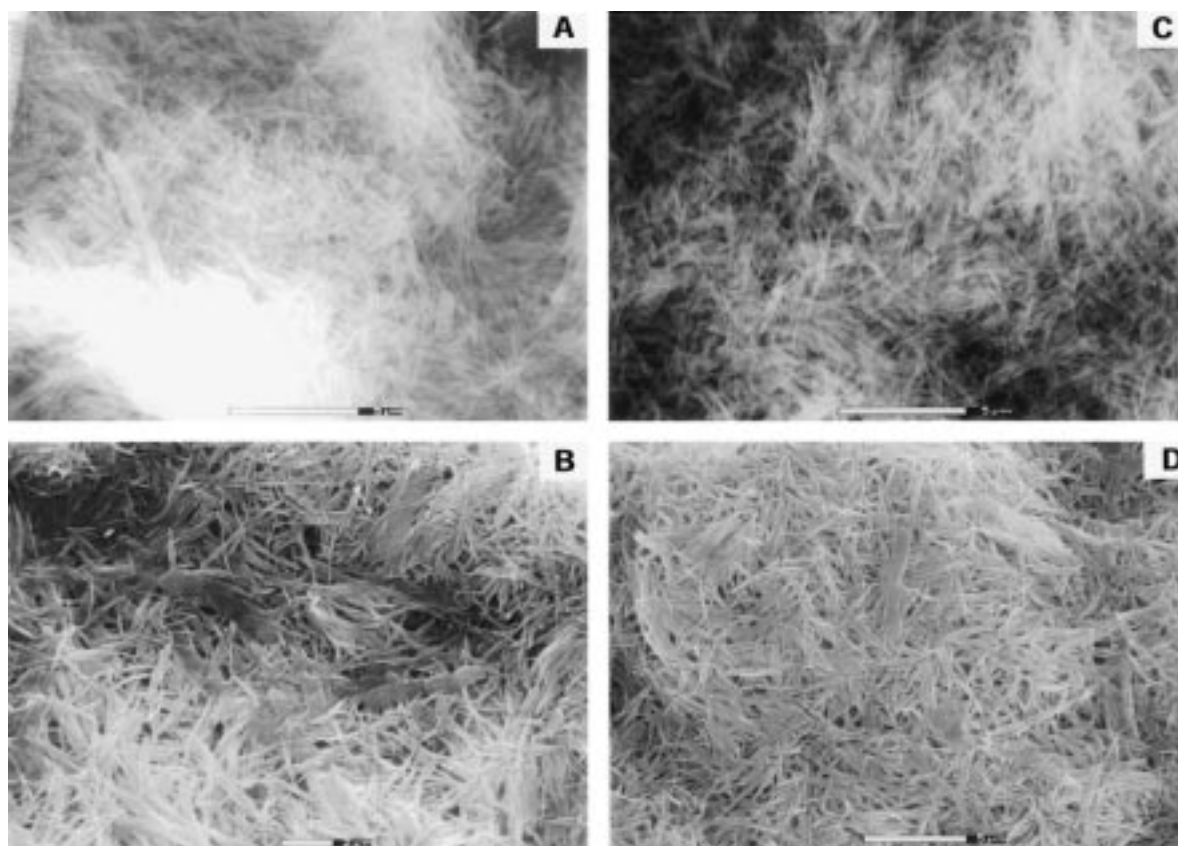
FIGURE 6. ESEM (**A** and **C**) and SEM (**B** and **D**) images of manganite after approximately 25% reduction of the manganite. These micrographs of wet samples (top panels), show visible, but somewhat obscured cells associated with the manganite. The bottom panels show samples from similar times of reduction. With these dried samples, the cells are more clearly seen among the clearly visible manganite particles. Bars = 5 μm.

B and D) eliminate this problem, and reveal the crystalline MnOOH with intimately associated bacteria.

After 75 to 80% total reduction (Figs. 7 and 8), bacterial cells are almost impossible to resolve using ESEM (Fig. 7, top panels). SEM imaging of identical fields (Figs. 7 and 8, bottom panels) demonstrates abundant bacteria growing on the metal oxide surface. Many cells are dividing, indicating an apparently healthy population. The biofilm of cells around the MnOOH particle is apparently only one cell layer thick, and cells appear to be in very close contact with the metal oxide. Figure 8 shows SEM images of the uninoculated manganite and three views of bacteria on the oxides at high magnification during a very late (>90%) stage of metal reduction.

DISCUSSION

We have examined the ability of *S. putrefaciens* strain MR-4 to catalyze the reduction of synthetic MnOOH prepared in the laboratory. Although the morphology of the manganite is decidedly different from other Mn^{4+} oxides (Myers and Nealson 1988a; Burdige et al. 1994), its reduction by *S. putrefaciens* was similar in many ways to

the microbial reduction of MnO_2. The reaction exhibited a pH optimum characteristic of an enzymatic reaction (e.g., a maximum around neutrality, with inhibition at high and low pH) and was inhibited by CCCP, mercuric chloride, and molecular oxygen. Temperature studies also showed a decided maximum around 35 °C. An increase in reaction rate of 2–3 for each 10 °C rise in temperature, followed by a rapid decrease once the denaturation temperature of the protein is reached is typical for a biochemically catalyzed reaction. For thermophiles or hyperthermophiles this maximum would be shifted upward, but the same general pattern would be seen.

Like the MnO_2 oxides previously studied (Burdige et al. 1992), reduction of MnOOH is mineral-surface limited; e.g., the addition of more mineral surface stimulates the rate of reaction, while the addition of more cells has very little effect on the reaction rate (Figs. 1 and 2). Burdige et al. (1992) showed that different Mn^{4+} oxides have significantly different rates of reduction, and that these differences are mostly due to differences in available surface area of the oxides. Not surprisingly, the rate of reduction of manganite was slower than the birnessite and faster than the pyrolusite, a coarsely crystalline oxide of
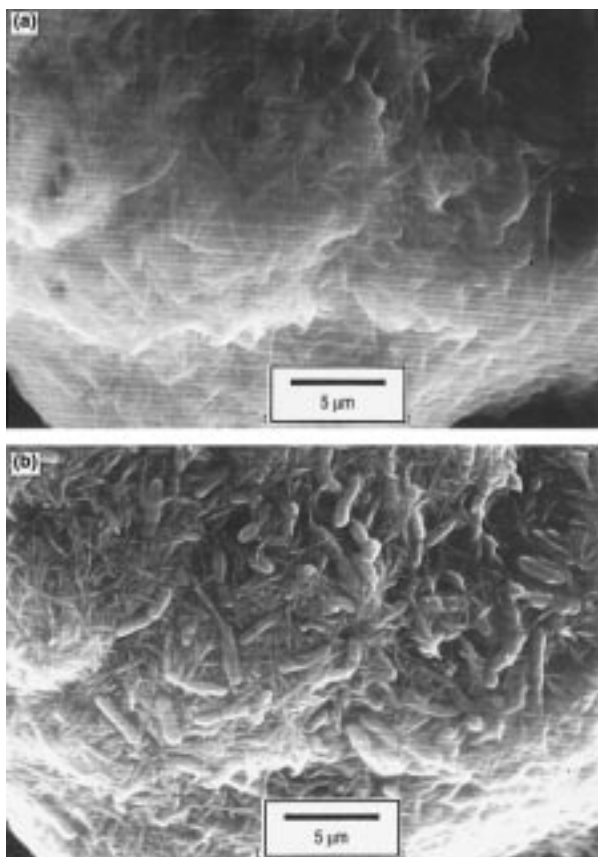
FIGURE 7. ESEM (**a**) and SEM (**b**) images of a manganite particle from a culture showing approximately 75% manganese reduction. The wet sample reveals that the manganite particles are so heavily coated with an unidentified layer that the individual cells are barely visible. Bar = 5 μm.

FIGURE 8. High-magnification SEM images of cells on the surface of manganite approximately 75% reduced. These samples were dried before imaging, but even with drying, a clear layer of cell-associated material (slime) is seen around the cells and around the manganite crystals. A = uninoculated manganite; B–D = images of manganite surface of bacteria-associated particle. Bar = 1 μm.

low surface area (Fig. 4) consistent with estimates of surface area made via comparisons of the relative surface areas of the minerals. However, until accurate surface area measurements of the oxides are made, it will not be possible to separate the factors responsible for these differences in rates; careful studies with manganese oxides of different chemistries, mineralogies, and surface areas will be required. With regard to surface area, Roden and Zachara (1996) studied the relationship between iron oxide reduction and surface area, concluding that rate and extent of iron oxide reduction were controlled by surface area and site concentration of the solid phase. It seems likely that the major controlling factor in solid metal reduction is surface area, with other factors such as crystal structure, morphology, free energy, and particle aggregation contributing to lesser degrees (Roden and Zachara 1996).

ESEM allows one to image at high magnification under atmospheric conditions, so that wet, and thus more "natural" samples can be viewed with the high resolution typical of standard SEM (Little et al. 1991). Using this technique, the needle-shaped crystals of the manganite
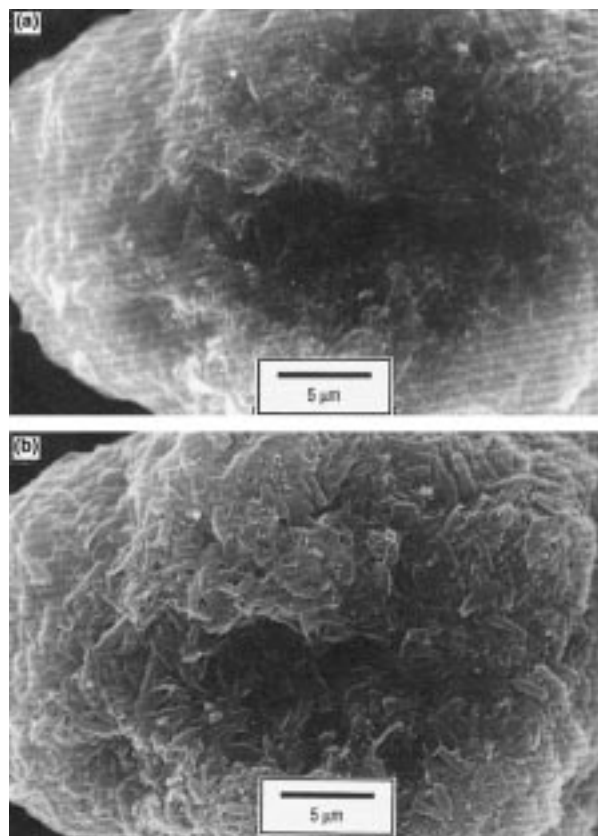
can be easily seen—presumably this is what a bacterium encounters as it approaches the oxide. As the manganite was colonized and reduced by *S. putrefaciens,* the surface of the metal oxide, as well as the cells populating the surface became obscured (Figs. 6–9). When the same samples were dried, gold coated, and viewed in the SEM, the bacteria were easily visible, suggesting that the thin film was removed or condensed by the process. The most likely candidate for an extracellular component so sensitive to solvent removal of water and drying is polysaccharide, but the chemical nature of the biofilm coating has not yet been determined. Typically microorganisms that colonize surfaces produce polymers and form a gel matrix that is central to the structural integrity of a biofilm (Little et al. 1991). The gel immobilizes water at the metal/biofilm interface and microbial activity within the matrix produces an interfacial chemistry that can be different from the bulk medium in pH, dissolved oxygen, and chemical (organic or inorganic) species. In some cases, bacterial metabolites within biofilms react with the substratum to produce localized phenomena. ESEM images
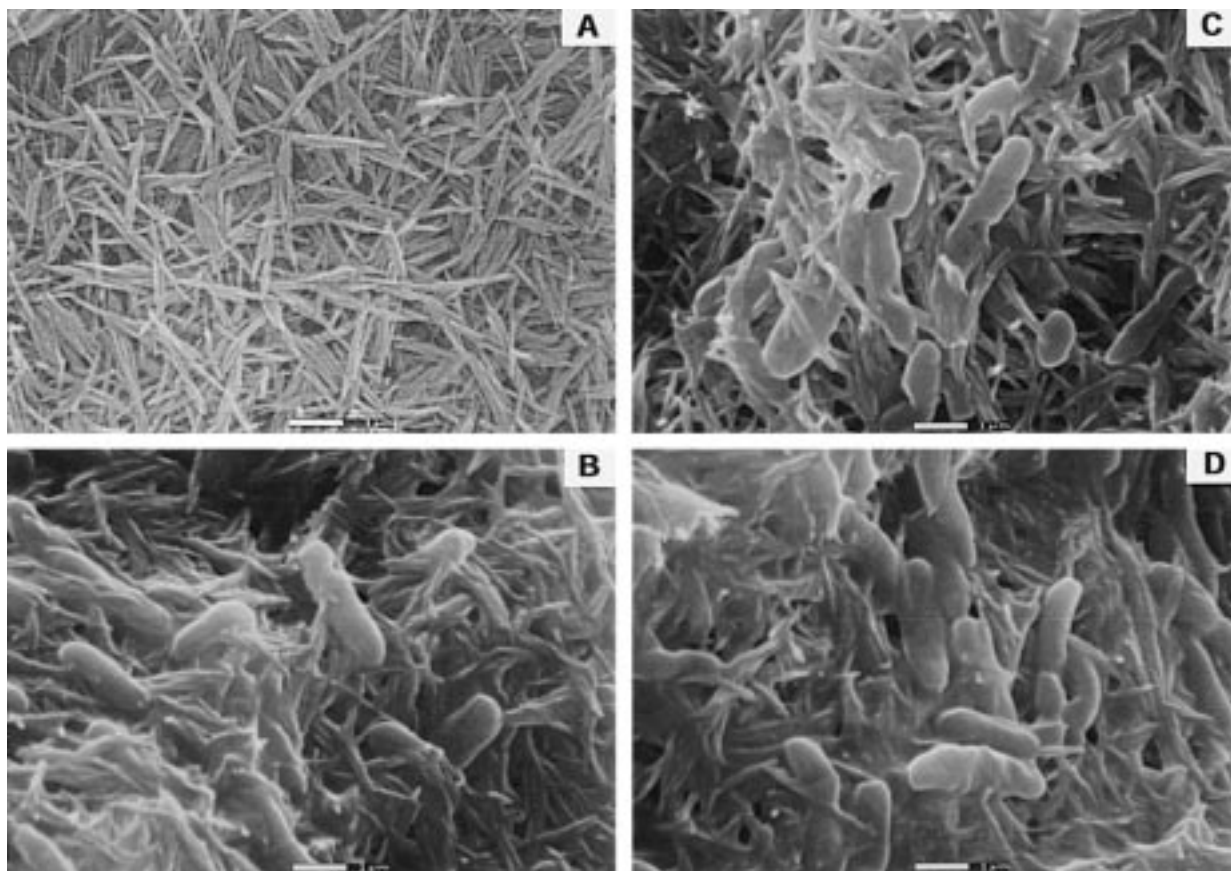
FIGURE 9. ESEM and SEM images of manganite particles taken from a culture showing approximately 90% manganese reduction. Even in the dried samples, it is difficult to resolve the cells, although upon close inspection, it can be seen that they are virtually continuous on the surface of the manganite.

of manganite exposed to *S. putrefaciens* indicated biofilm formation within 24–48 h. Bacterial cells were enmeshed within the gel matrix so that it was impossible to image individual cells. After solvent removal of water and drying, much of the matrix material from the biofilm was removed or collapsed, exposing bacterial cells. The presence of biofilms on minerals during metal reduction has not been previously documented, and the role of biofilms in metal reduction has not been resolved. Although the fine structure of the bacteria/metal relationship has not been resolved by using ESEM analyses, it is clear that the bacteria are intimately associated with the metal surface, and resolution of these intimate relationships may well lend insights into the mechanism(s) by which bacteria populate and dissolve solid metal oxides.

REFERENCES CITED

Amos, W.B., White, J.G., and Fordham, M. (1987) Use of confocal imaging in the study of biological structures. Applied Optics, 26, 3239–3243.

Bricker, O. (1965) Some stability relations in the system Mn-O$_2$-H$_2$O at 25° and one atmosphere total pressure. American Mineralogist, 50, 296–345.

Burdige, D.J., Dhakar, S.P., and Nealson, K. (1992) Effects of manganese oxide mineralogy on microbial and chemical manganese reduction. Geomicrobiology Journal, 10, 27–48.

Clesceri, L.S., Greenberg, A.E., and Eaton, A.D. (1989) Standard methods for the examination of water and wastewater, p. 9-39–9-40. American Public Health Association, Washington, D.C.

Hewett, D.F. (1966) Stratified deposits of the oxides and carbonates of manganese. Economic Geology, 61, 431–461.

Hewett, D.F. and Fleischer, M. (1960) Deposits of the manganese oxides. Economic Geology, 55, 1–55.

Junta, J.L. and Hochella, M.F. (1994) Manganese (II) oxidation at mineral surfaces: a microscopic and spectroscopic study. Geochimica Cosmochimica Acta, 58, 4985–4999.

Kostka, J.E., Luther, G.W. III, and Nealson, K.H. (1995) Chemical and biological reduction of Mn(III)-pyrophosphate complexes: potential importance of dissolved Mn(III) as an environmental oxidant. Geochimica Cosmochimica Acta, 59, 885–894.

Little, B., Wagner, P., Ray, R., and Sheetz, R. (1991) Biofilms: an ESEM evaluation of artifacts introduced during SEM preparation. Journal of Industrial Microbiology, 8, 213–222.

Moser, D. and Nealson, K.H. (1996) Growth of Shewanella putrefaciens on elemental sulfur as an electron acceptor. Applied and Environmental Microbiology, 62, 2100–2105.

Myers, C. and Nealson, K.H. (1988a) Bacterial manganese. reduction and growth with manganese oxide as the sole electron acceptor. Science, 240, 1319–1321.

————(1988b) Microbial reduction of manganese oxides: Interactions with iron and sulfur. Geochimica Cosmochimica Acta, 52, 2727–2732.

Roden, E.E. and Zachara, J. (1996) Microbial reduction of crystalline iron(III) oxides: Influence of oxide surface area and potential for cell growth. Environmental Science and Technology, 30, 1618–1628.

Stone, A.T. and Morgan, J.J. (1984a) Reduction and dissolution of manganese(III) and manganese(IV) oxides by organics. 1. Reaction with hydroquinone. Environmental Science and Technology, 18, 450–456.

————(1984b) Reduction and dissolution of manganese(III) and manganese(IV) by organics. II. Survey of the reactivity of organics. Environmental Science and Technology, 18, 617–624.

Stumm, W. and Giovanoli, R. (1976) On the nature of particulate manganese in simulated lake waters. Chimia, 30, 423–425.

Xyla, L., Sulzberger, B., Luther, G.W., Hering, J.G., VanCapellan, P., and Stumm, W. (1992) Reduction dissolution of manganese (III,IV) (hydr)oxides by oxalate: the effect of pH and light. Langmuir, 8, 95–103.